Cytometry
PART A
Journal of the International Society for Advancement of Cytometry

Enhanced FRET Contrast in Lifetime Imaging

Corentin Spriet,[1] Dave Trinel,[1] Franck Riquet,[1] Bernard Vandenbunder,[1] Yves Usson,[2] Laurent Heliot[1]*

[1]Lille University of Science and Technology, Interdisciplinary Research Institute, CNRS USR 3078, Biophotonic team, 1 rue Prf. Calmette, 59021 Lille cedex, France

[2]Universitè Joseph Fourier, Laboratoire TIMC-IMAG; 2 CNRS, UMR5525, La Tronche F38706, France

Received 22 January 2008;
Revision Received 25 March 2008;
Accepted 21 April 2008

Present address of Corentin Spriet: B040, Biophysik der Macromolekule, DKFZ, Im neuenheimer Feld 280,D-69120, Heidelberg, Germany.

Grant sponsors: CNRS (MRCT), ANR-05-MIIM-042; Règion Nord-Pas-de-Calais, FEDER: La Ligue contre le Cancer; ARC; Leica Microsystems.

*Correspondence to: Laurent Heliot, Interdisciplinary Research Institute, 1 rue du professeur Calmette, Bp 447, 59021, Lille Cedex France.

Email: Laurent.heliot@ibl.fr

Published online 21 May 2008 in Wiley InterScience (www.interscience.wiley.com)

DOI: 10.1002/cyto.a.20581

Abstract

In combination with two photon excitation, FLIM is currently one of the best techniques to quantitatively study the subcellular localization of protein–protein interactions in living cells. An appropriate analysis procedure is crucial to obtain reliable results. TCSPC is an accurate method to measure FLIM. It is however an indirect process that requires photon decay curve fitting, using an exponential decay equation. Although choosing the number of exponential terms is essential, it is labor-intensive and time consuming. Therefore, a mono-model is usually applied to a whole image. Here we propose an algorithm, named Liχ, allowing pixel by pixel analysis based on the $\Delta\chi^2$ value. Liχ was validated using simulated photon decay curves with known lifetimes and proportions. It showed a high robustness for decay curves with more than 10^3 photons. When applied to lifetime images acquired from living cells, it resulted in a more realistic representation of the interaction maps. We developed an easy-to-use procedure for multi-model FLIM analysis, which enables optimized FRET quantification for all interaction texture studies, and is especially suitable to avoid the classical misinterpretation of heterogeneous samples.

Key terms

lifetime; FLIM; TCSPC; FRET; curve fitting; model choice; protein–protein interactions; living cells

BIOCHEMICAL assays can identify potential protein–protein interactions in cell extracts, but studying these interactions in living cells is a more challenging task. The most promising approach for the measurement of molecular interaction dynamics exploits the energy transfer between fluorophores over short distances (Fluorescence Resonance Energy Transfer; FRET) (1). This transfer occurs only if both molecules are in close proximity to one another (typically less than 10 nm) (2).

Several strategies are used to obtain this measurement which are mainly based on fluorescence intensity (3), anisotropy (4), and lifetime (5) measurements. The latter is rather accurate, especially when using a Time Correlated Single Photon Counting (TCSPC) system (6) and an instrumental setup with a narrow Instrumental Response Function (IRF) (7). This spectroscopy technique can either be used for the measurement of fluorescence lifetime of selected areas or for the acquisition of complete images; in which case it is referred to as FLIM (Fluorescence lifetime imaging microscopy). TCSPC is an indirect method that allows determination of the fluorescence lifetime species by fitting measured photon decay curves using the following equation:

$$y = \left(\sum_{i=1}^{n} a_i \cdot e^{-t/\tau_i} + b \right) \otimes \mathrm{IRF} \qquad (1)$$

With "b" the background level, "IRF", IRF of the acquisition system, "i" an index associated with each exponential, "a" the proportion of each component and "τ" the corresponding lifetime.

ISAC
International Society for Advancement of Cytometry

A mean fluorescence lifetime defined as in Eq. (2) is used to facilitate comparison between experiments (8),

$$\tau_m = \frac{\sum_i a_i.\tau}{\sum_i a_i} \tag{2}$$

With "a" the proportion and "τ" the lifetime of each fluorescent component.

In general, fluorescence lifetime analysis is performed based on the Least squares method relying on the iterative minimization of the χ^2 parameter (9,10). Parameters that according to Marquardt (11) describe the difference between the model and the measured data are:

$$\chi^2_{\min} = \min_{a_j,\tau_j} \frac{\frac{1}{2}\sum_{i=1}^{n} f_i(a_j.\tau_j)^2}{(\sqrt{\text{variance}})^2} \tag{3}$$

and

$$f_i(a_j,\tau_j) = V_i - \left(b + \text{IRF} \otimes \sum_j a_j.e^{\left(\frac{-t}{\tau_j}\right)}\right) \tag{4}$$

With "i" the time channel, "V" the photon number, "b" the background, "IRF", IRF of our system, "j" an index associated with each exponential, "a" the proportion of each component and "τ" the corresponding lifetime.

Using a least squares based fit procedure implies the choice of the fluorescence species used in Eq. (1). This choice is usually achieved based on the fit curve residual distribution.

To accurately calculate the fluorescence lifetime, the choice of "n" in Eq. (1) is essential as demonstrated in Figure 1. On one hand, a missing exponential term leads to an overestimation of fluorescence lifetime (Fig. 1A). On the other hand, an overestimation of the model's degree of freedom, i.e. exponential terms results in instability of the fitting algorithm (12), and so, in higher dispersion of estimated lifetimes (Fig. 1B). The Occam's or Ockham's razor (13), also referred to as parsimony law, states a preference for simple theories. Consequently, the fit model that describes the photon decay curve with the lowest number of exponentials is preferred.

The choice of the optimal fit model based on the residual statistics has a strong theoretical foundation in literature of both statistics and information theory fields (14,15). However, the information that is crucial to apply this theory is not easily accessible from the FLIM analysis software. Moreover, it cannot be directly used for the generation of lifetime images.

In this article, we describe an easy-to-use analysis procedure based on the χ^2 variation that allows for best model choice on a pixel-by-pixel basis. It uses information available in all FLIM analysis systems without complex modification of the fitting algorithm. We demonstrate its robustness throughout the analysis of series of simulated photons decay curves. We then show the improvement gained when applied to FRET investigation in living cells.

Materials and Methods

Plasmids

The memb-eGFP-mCherry was constructed using the memb-mCherry (16) which is derived from the PM-eGFP (17). We inserted, upstream of the mCherry coding sequence using standard molecular biological techniques, a hydrophilic linker (18) and the necessary restriction enzyme cutting sites for the in-frame subcloning of the eGFP fragment derived from the pEGFP-1 (Clontech). Plasmid clones were propagated in XL1 blue (Stratagene) and checked by sequencing.

For Rab6 and Rab11 plasmid constructs see (19) and (20), respectively.

Cell Culture and Transfection

A *HeLa* stable cell line expressing eGFP was generated after transfection of 1 μg of pEGFP-1, using 3 μl of transfectin (Bio-Rad). Clones were selected by repeated flow cytometry sorting.

HeLa cells were grown in plastic flasks at 37°C in 5% CO_2 in Dulbecco's modified Eagle's medium (GIBCO/BRL) supplemented with 10% Fetal Calf Serum, 4 mM L-glutamine and 5 mM sodium pyruvate. Cells were plated on 32 mm diameter glass coverslips 12 h prior to transfection. One hour before transfection, culture medium was removed and replaced with culture medium containing 100 units/ml penicillin/streptomycin. Transient transfections of Rab plasmids were performed by calcium phosphate method on native *HeLa* cells (21).

FuGENE HD was used for the transfection of memb-eGFP-mCherry on *HeLa* cells stably expressing eGFP. Observations were conducted 24 h after transfection. For FLIM imaging, culture medium was replaced by L15 medium (Invitrogen) for pH stabilization during experiments.

Two-Photon Fluorescence Lifetime Microscopy

The Time Correlated Single Photon Counting (TCSPC) FLIM system was built around a Leica SP2 confocal Microscope (Leica Microsystems), a pulsed laser source (Ti: Sapphire with a 5 W Verdi pump laser, Mira900-F, Coherent Inc.), a detector with high temporal resolution (MCP PMT model R3809U-52, Hamamatsu) and a dedicated photon-counting and timing electronic card (SPC 730 TCSPC card, Becker & Hickl). For more details about the system implementation and characterization, see (7).

Monte Carlo Simulation of Photon Decay Curves

To assess the curve fitting estimation methods, a number of data set or photon histograms with controlled/known parameters were generated using a Monte Carlo approach.

In brief, the method consisted of drawing in a random number generator as many discrete time values as the desired number of photons in the final data set. The density probability function of the random generator corresponded to the theoretical decay curve of the simulated data set. To generate a data set that mimics the instrument data acquisition characteristics, we added uniformly distributed false photons to recapitulate instrument noise. We also took into account that the tail of photon decay curves could exceed laser pulse period and consequently some photons might be collected in the wrong time channels (data wrapping). This was solved by implementing a modulo function that wrapped around the generated data set.

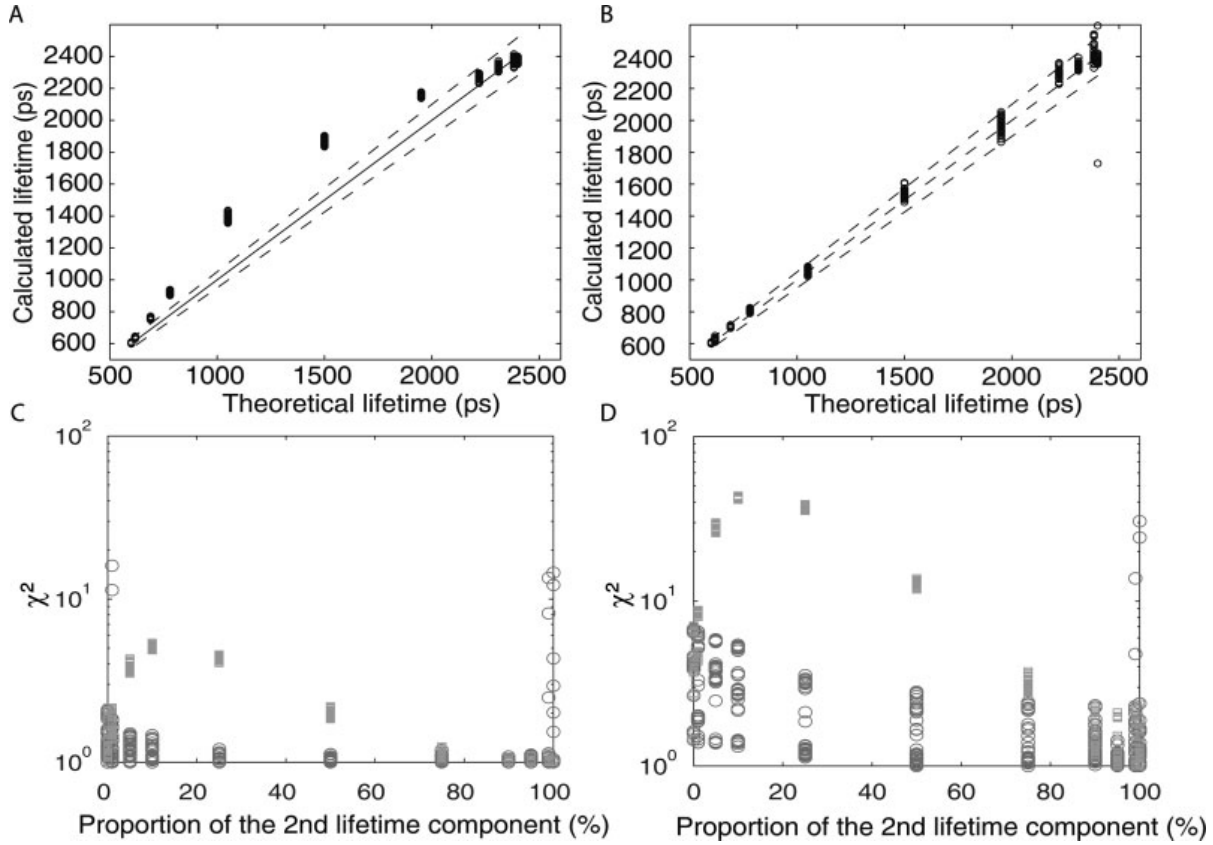

Figure 1. Comparison between mean lifetimes obtained from a mono-exponential **(A)** or a bi-exponential fit **(B)** of simulated data sets, compared with theoretical values. Simulations were performed on a mix of $\tau 1 = 0.6$ ns and $\tau 2 = 2.4$ ns with different proportions (0, 1, 5, 10, 25, 50, 75, 95, 99, and 100%) for a total simulated photon number of 10^5 and a signal to noise ratio of 100. Straight lines correspond to a perfect correspondence between simulated and fitted lifetimes. Dotted lines correspond to 5% error. **(C, D)**, χ^2 values obtained from the previously described simulations either after mono-exponential (green squares) or bi-exponential (red open circles) fit for a total photon number of 10^5 (C) and 10^6 (D) photons as a function of the second lifetime component proportion. 30 simulations per condition.

The controlled parameters were:

- n the number of time channels (1024 bins) in the photon histogram,
- t_h the time length of a histogram bin, r the pulse repetition period (12 ns),
- t_p the start of the pulse,
- N the total number of photons,
- IRF the instrument response function,
- m the number of exponential decay functions f_i such that $f_i(t) = \eta_i \exp(-(t-t_p)/\tau_i)$ when $t \geq t_p$ and $f_i(t) = 0$ otherwise, with η_i the proportion and τ_i the decay parameter,
- N_f the number of false photons due to instrument noise.

Let's call D, the decay curve such that $D(t) = \text{IRF} \otimes \sum_1^m f_i(t)$ where $\otimes$ denotes convolution.

The algorithm for data sets generation was the following:

1. Set all histogram bins to zero and variable count to zero,
2. Within a range from 0 to 1, draw a value x from a random number generator with an uniform probability,
3. Find the t_x value so that the normalised integral of D from 0 to t_x equals x,
4. Calculate the bin number $b \leftarrow \text{integer}[(t_x \bmod r)/t_h]$, where mod denotes modulo,
5. If $b < n$ then add a photon in bin b of the photon histogram and increment count,
6. Repeat steps 2 to 5 until the counter equals N-N_f.
7. Within a range from 0 to 1023, draw an integer number k from a random number generator with a uniform probability,
8. Add a photon in bin k of the photon histogram and increment count,
9. Repeat steps 7 to 8 until count equals N.

Photon Decay Curve Analysis

Lifetime images were analyzed by fitting data with a mono and bi-exponential function [see Eq. (1)] using the SPC Image software (Becker & Hickl). First, for each point of the curve, $f_i(a_i,\tau_j)$ was calculated according to Eq. (4).

The software then iteratively modifies a_j and τ_j in order to minimize the χ^2 parameter [Eq. (3)].

Following analysis, fluorescence lifetimes, proportions and χ^2 values are exported in ASCII format and processed using the MFS homemade ImageJ plug-in (22), available as a freeware.

Results

Our aim was to optimize the fitting method, based on the Occam's razor or parsimony law, which implies that an additional exponential in Eq. (1) is only needed if it generates a significantly improved solution. Although the natural tendency of a fitting algorithm is to increase the number of variables in response to the system's fluctuation, it is detrimental to the overall understanding of the system. Therefore, implementing a fitting quality criterion is essential and would render both data analysis and biological interpretation, accurate and relevant, respectively. Here, we propose to ground this fitting quality criterion to the χ^2 variation as a function of the incremental number of exponential terms.

We deliberately limited our demonstration to the choice between a mono and bi-exponential model since it is representative of most interaction texture studies in living cells. It could however be easily extended to a higher number of exponentials terms.

$\Delta\chi^2$ Definition and Threshold Determination

Although the χ^2 value is dependent on both the relevance of the exponential model and the total photon number, a threshold value may not be directly generated from these parameters to choose the best model. However, the difference between the χ^2 after mono-exponential and bi-exponential fit is only derived from the number of species included in the model, as illustrated in Figure 2A. For instance, inaccuracy linked to proper IRF estimation and convolution is the same regardless of the number of species in the model. Thus, the difference between χ^2 after mono-exponential and bi-exponential fit results from the relevant usage of each exponential model.

We next proposed to use the variation termed $\Delta\chi^2$ in Eq. (5) as a fitting quality criterion in order to ascribe the most adapted exponential model.

$$\Delta\chi^2 = \frac{((\chi_m^2 - 1) - (\chi_b^2 - 1)).100}{(\chi_m^2 - 1)} \qquad (5)$$

With "χ_m^2" and "χ_b^2" (2) being χ^2 value obtained respectively after a mono-exponential or a bi-exponential fit applied to the photon decay curve.

To test the relevance of this parameter as a fitting quality criterion, we performed Monte Carlo simulations of photon decay curves with different total photon numbers and exponential component proportions (see Materials and Methods section). For each of these curves, the $\Delta\chi^2$ was calculated. We then tested different values of $\Delta\chi^2$ as a discriminating criterion to determine the optimal fit model. Results from these simulations are summarized in Table 1.

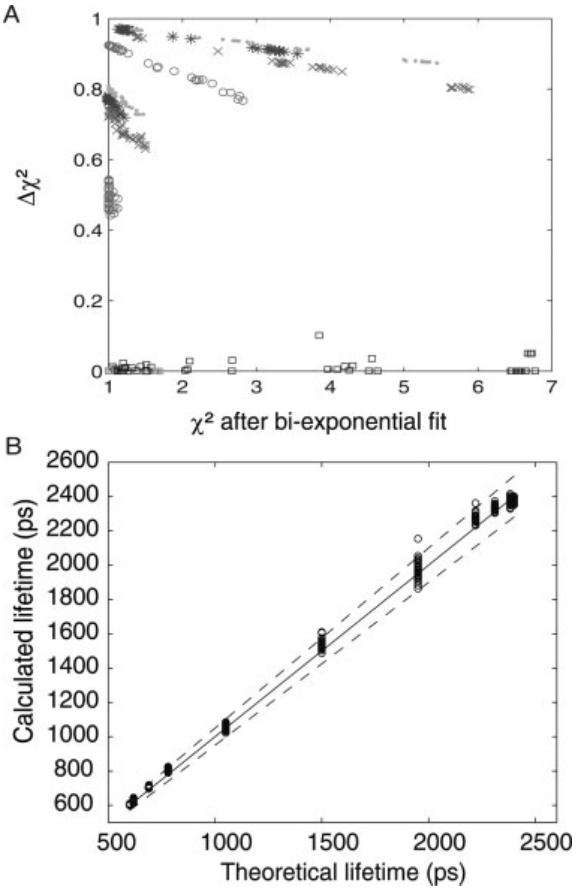

Figure 2. Estimation of a 20% $\Delta\chi^2$ threshold in decay curve analysis with variable lifetime contributions. **(A)** behavior of χ^2 values after bi-exponential fit and $\Delta\chi^2$ from curves presented in Figure 1. Curves are either mono-exponential (squares 100% of τ = 0.6 ns, green or τ = 2.4 ns, black) or bi-exponential (purple crosses, 5% of τ = 0.6 ns; cyan dots, 10% of τ = 0.6 ns; blue asterisks, 25% of τ = 0.6 ns; red open circles, 50% of τ = 0.6 ns. The remaining % are τ = 2.4 ns contribution). Total photon number is 10^5 or 10^6 photons. **(B)** analysis performed on data presented in Figure 1 based on a $\Delta\chi^2$ threshold set to 20%. Simulations were performed on a mix of $\tau 1$ = 0.6 ns and $\tau 2$ = 2.4 ns with different proportions for a total simulated photon number of 10^5 and a signal to noise ratio of 100. 30 simulations per condition.

To accurately quantify the fluorescence lifetime, the following requirements should be fulfilled: a minimum photon number per curve and an appropriate $\Delta\chi^2$ threshold. When setting the $\Delta\chi^2$ threshold to 20%, errors could be found in less than 2% and 12% of the cases for acquisition respectively collecting at least 10^5 and 10^4 photons per curve. When considering the usual amount of photons collected during FLIM acquisitions on living cells, the above $\Delta\chi^2$ threshold value leads to both optimal accuracy and reproducibility.

Robustness of $\Delta\chi^2$ as a Discriminating Factor

To further investigate the relevance of the $\Delta\chi^2$ threshold, we tested it on a series of photon decay curves, generated via

Table 1. Frequency of occurrence when the wrong model is selected; depending on the number of photons and $\Delta\chi^2$ threshold [Color table can be viewed in the online issue, which is available at www.interscience.wiley.com.]

Nbr of photons/$\Delta\chi^2$	10,0	20,0	30,0	40,0	50,0	90,0	Error (%):
1.000	35,7	34,8	34,3	34,6	34,9	45,0	>20
10.000	13,7	12,0	11,9	12,1	12,9	27,3	<20
100.000	4,2	1,7	2,3	2,7	4,7	26,3	<5
1.000.000	1,7	0,0	0,0	0,0	3,3	32,7	<2

Simulations were performed on a mix of $\tau1 = 0.6$ ns and $\tau2 = 2.4$ ns with different proportions (0, 25, 50, 75, and 100%) and a noise ratio of 100. 30 simulations per condion.

Monte Carlo simulations, with variable lifetimes, proportions and signal-to-noise ratios values.

Firstly, we performed an extensive study by mimicking different behaviors of fluorophores solutions through the mixture of simulated fluorescent lifetimes of $\tau1 = 0.6$ ns and $\tau2 = 2.4$ ns as shown in Figure 2. These values were chosen because they are representative of the ones obtained in classical FRET studies, using the most common FRET pairs (i.e. CFP-YFP, GFP-mRFP, and their variants). The first step was to assess whether any advantages could be drawn from a $\Delta\chi^2$ study over a regular χ^2 study. Data from Figure 2A clearly showed that no χ^2 value could be found to classify experiments between mono-exponential and bi-exponential curves. However, all mono-exponential curves exhibited a $\Delta\chi^2$ below 10%, while bi-exponential curves resulted in a $\Delta\chi^2$ greater than 40%. Thus the previously chosen fitting quality criterion, $\Delta\chi^2$, set to 20% was hereby validated since it provided the optimal exponential model choice. Confirmation came from Figure 2B where fluorescence lifetimes obtained after a model choice based on a $\Delta\chi^2 = 20\%$ were consistent with expected theoretical lifetimes. In addition, the calculated mean lifetime benefited from both, mono-exponential fitting stability, and bi-exponential accuracy.

Secondly, we determined the robustness of the $\Delta\chi^2$ criterion on simulated photon decay curves with variable lifetimes and signal to noise ratios.

- 50%/50% mixes of different lifetime (Figs. 3A1 and 3A2)
- 50%/50% of $\tau1 = 0.6$ ns and $\tau2 = 2.4$ ns with different signal to noise ratio (Figs. 3B1 and 3B2).

In all cases, $\Delta\chi^2$ enabled the optimal model choice while keeping well above the 20% threshold value. The robustness of the fitting quality criterion was validated, and applied to live cell FRET measurements in classical fitting configurations encountered in FLIM experiments.

Liχ Algorithm

The different characterization steps enabled us to propose an algorithm, Liχ, based on $\Delta\chi^2$ value, which is applicable to lifetime images. It is integrated in MFS, a Java plug-in for ImageJ.

Liχ is divided into four steps:

- The photons/pixel threshold should be set to 10^3 to exclude background pixels.
- The photons/pixel threshold should be set to 10^4. Based on both simulations and theory, only a mono-exponential fitting is reliable (17).
- Then, for each remaining pixel, the $\Delta\chi^2$ is calculated [Eq. (5)]: If $\Delta\chi^2$ is less than 20%, a mono-exponential fitting is chosen. If $\Delta\chi^2$ is more than 20%, a bi-exponential is more reliable.
- Finally, fluorescence lifetime values from previous steps are gathered into a single lifetime image.

Extending Liχ to more than two exponentials is easily feasible. In order to do so, one needs to fix a new threshold value for each additional exponential term and to calculate the $\Delta\chi^2$ between "n" and "$n + 1$" exponentials. Then, every image calculated from each cycle should be gathered into one.

Application to Enhance Live Cell Lifetime Imaging

Upon Liχ validation with Monte Carlo simulated photon decay curves, we tested the algorithm by analyzing *HeLa* cells stably expressing eGFP and transiently transfected with a membrane targeted construct expressing eGFP and mCherry in tandem (see MATERIALS AND METHODS section for details). This plasmid was used as positive FRET reference (Fig. 4).

This experiment enabled the acquisition of images exhibiting an heterogeneous photon count, with mono-exponential areas, characterized by signal in the green channel only (Fig. 4A, cell No. 1), and bi-exponential areas characterized by signal from both green and red channels (Fig. 4C, cell No. 2 and No. 3). When considering the fitting residuals (Fig. 4B), the random distribution after mono-exponential fit obtained in cell No. 1 and No. 2 confirmed the relevance of such a model choice while the non-random distribution obtained from cell No. 3 suggested a lack of exponential species in the model. The automated Liχ based fit model choice presented in Figure 4D revealed an analyzed image that consistently took into account the above observation: a mono-exponential fit

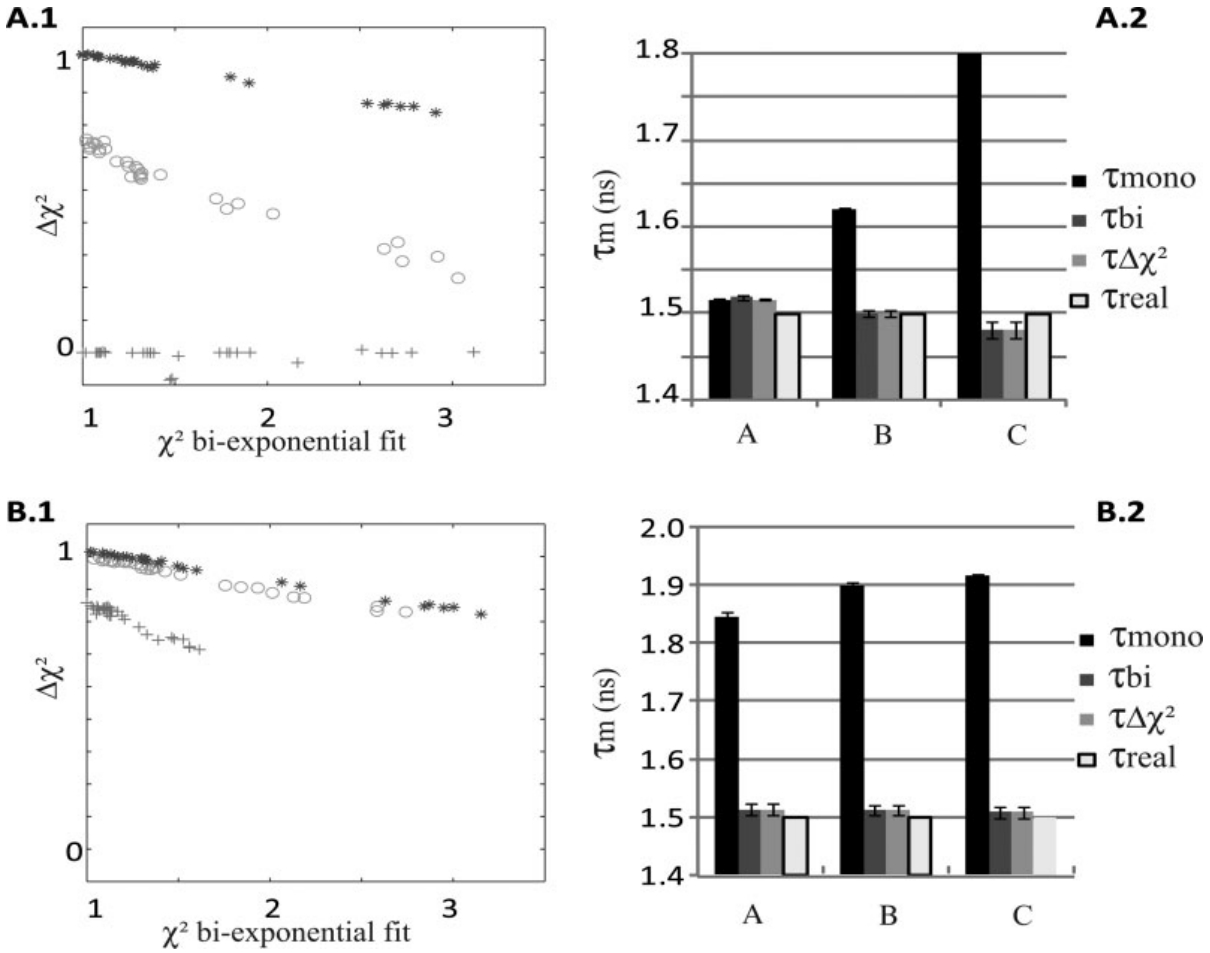

Figure 3. Estimation of a 20% $\Delta\chi^2$ threshold in decay curve analysis with 50%/50% of different contributing lifetimes **(A)**, respectively 1.6/1.4 ns (red crosses), 2.0/1.0 ns (green circles) and 2.4/0.6 ns (blue asterisks); or different signal to noise ratio (S/N) **(B)**, respectively S/N = 1 (red cross), 10 (green open circle) or 100 (blue asterisk). **(1)**, behavior of $\Delta\chi^2$ as a function of χ^2 values after bi-exponential **(2)**, fluorescence lifetimes obtained after a mono-exponential fit (τmono), a bi-exponential fit (τbi), fit using model determined by a $\Delta\chi^2$ of 20% ($\tau\Delta\chi^2$), or calculated from the lifetime and proportion used for simulation (τreal). 30 simulations per condition.

was applied to cell No. 1 and No. 2, and a bi-exponential fit to cell No. 3. Most important, these results were achieved without the need for a fastidious pixel by pixel manual inspection of the fitting residuals. The resulting contrasted fluorescence lifetime variation image is presented in Figure 4E.

Finally, we applied Liχ to the analysis of *HeLa* cells co-expressing Rab6A-CFP, Rab11A-YFP and a non-tagged Rab6IP1 (21). These proteins are localized in the dispersed Golgi apparatus upon nocodazol treatment (Fig. 5). Interactions between Rab6A and Rab11 triggered by Rab6IP1, which occur only in some vacuoles, provide a good example of interactions heterogeneity in living cells.

A classical mono-model fitting (mono or bi-exponential model applied to the whole image) yielded fluorescence lifetime images shown in Figures 5A and 5B, resulting in errors in interaction interpretations. However, using our algorithm, we generated a fluorescence lifetime image (Fig. 5C), containing areas with one or two fluorescent species. The lifetime distribution given for each pixel (Fig. 5D) underlined the mis-interpretation resulting from a mono-model analysis. Indeed, the mono-exponential analysis showed a single population, where the bi-exponential model exhibited a bimodal distribution but with wrong proportions. Figures 5E and 5F present photon decay curves (blue) with associated mono-exponential (Figs. $5E_1$ and $5F_1$) or bi-exponential (Fig. $5E_2$ and $5F_2$) fitting curves (red) and fitting residuals (black). Photon decay curves presented in Figure 5E were extracted from a bi-exponential area in accordance with both Liχ and fitting residuals analysis (red arrow). Obviously, there was a degree of freedom missing in Eq. (1) after a mono-exponential fit (Fig. $5E_1$) when compared to a bi-exponential fit (Fig. $5E_2$). In contrast, photon decay curves, gathered from a mono-exponential area according to $\Delta\chi^2$ (green arrow), were perfectly adjusted with a mono-exponential model (Fig. $5F_1$), while a bi-exponential

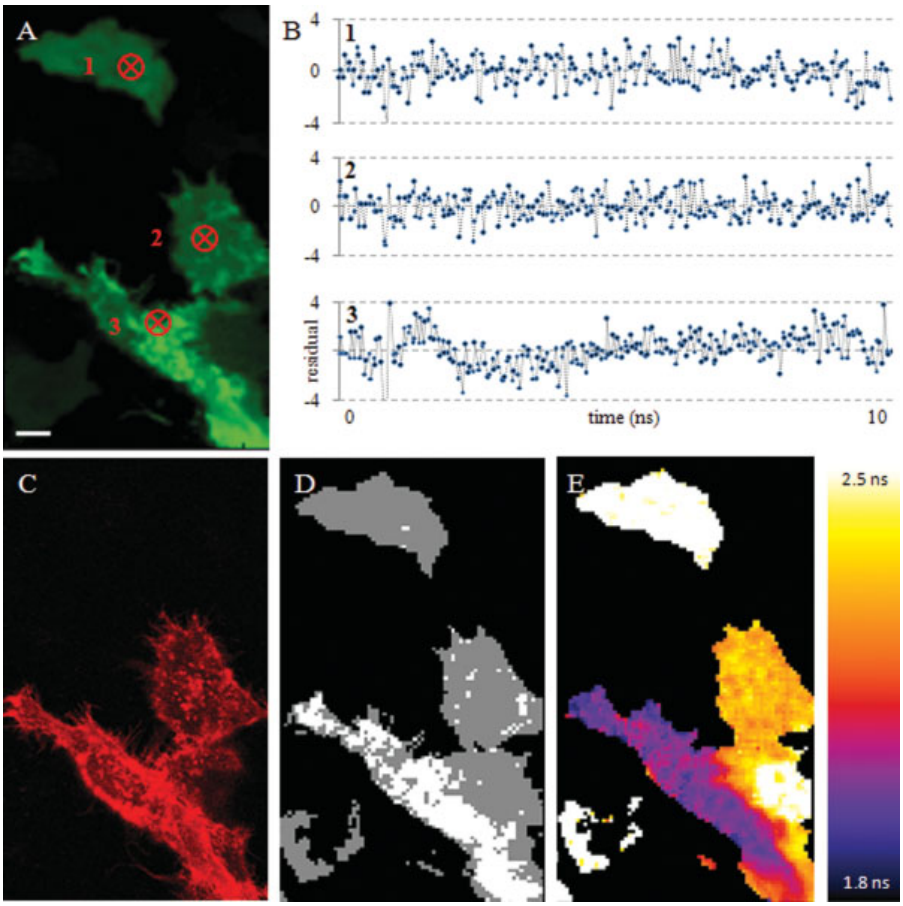

Figure 4. $\Delta\chi^2$ based analysis of *HeLa* cells expressing e-GFP and memb-eGFP-mCherry. **(A)** Two Photon image of eGFP [Ex: 880 nm, Em: 400–435 nm], scale bar 10 μm. **(B)** fitting residuals obtained after a mono-exponential fit of curves extracted from the pixels indicated in (A). **(C)** Confocal image of channel [Ex: 543 nm, Em: 580–660 nm] corresponding to mCherry fluorescence emission. **(D)** Model choice based on Liχ, background (black), mono-exponential choice (gray) and bi-exponential choice (white). **(E)** Fluorescence lifetime image obtained through Liχ-based analysis.

fit improved neither the χ^2 value nor the fitting residual (Fig. 5F$_2$).

Discussion

Fluorescence lifetime imaging is a powerful tool for localizing interactions in living cells. However, interaction texture studies become increasingly interesting in the case of heterogeneity, which implies different behavior of photon decay curves. FLIM analysis software, such as SPCImage, only proposes a mono-model analysis, which dramatically decreases the lifetime contrast and leads to erroneous interpretation of FRET measurements. Our algorithm, Liχ, which is based on the calculation of the $\Delta\chi^2$ parameter, greatly improves the information that can be extracted from lifetime images.

Optimal conditions were reached, for both simulated and measured photon decay curves, when the $\Delta\chi^2$ threshold was set to 20% and the number of photons was greater than 10^3 photons per curve. In this context, the sole obstacle to information extraction is the potential application of a bi-exponential analysis to photon decay curves with poor statistics. This became quite obvious upon analysis of individual lifetimes of either mix with low contribution of the longest lifetime (less than 25% of the long lifetime component in Fig. 1), or mixtures of simulated fluorescence species with respective lifetimes of 1.6 ns and 1.4 ns. A mono-exponential equation offered the best result as a bi-exponential fit was not able to extract the appropriate lifetime and proportion and only induced a higher instability of the fitting algorithm.

Such an example is provided by cell No. 2 (Fig. 4). Indeed, the presence of both eGFP (stable cell line) and memb-eGFP-mCherry (signal in the red channel) implied the presence of two fluorescent species, and thus suggested a bi-exponential behavior. Considering the mean photon number per curves ($\sim 2.10^4$), and in view of the fitting residual and Liχ based choice, a mono-exponential fit was more appropriate in this context. In addition, a bi-exponential fit

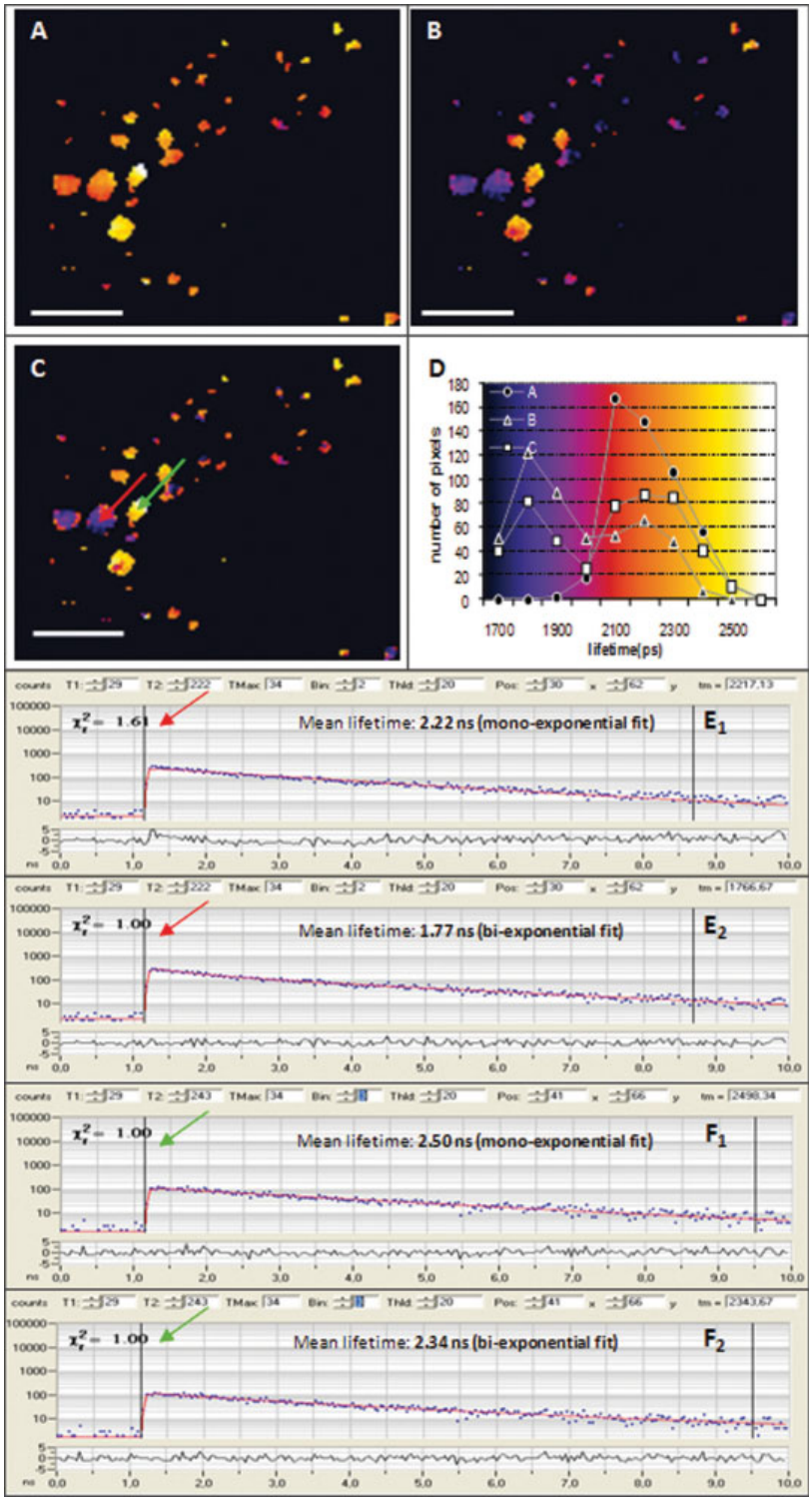

Figure 5. $\Delta\chi^2$-based analysis of *HeLa* cell expressing two different Rab proteins tagged with CFP or YFP after nocodazol treatment. Fluorescence lifetime obtained assuming a mono-exponential decay **(A)**, a bi-exponential decay **(B)** or after analysis based on a $\Delta\chi^2$ threshold of 20% using the MFS ImageJ plug-in **(C)**. **(D)** Lifetime distribution in A, B, C, and associated Look Up Table. **(E)**, **(F)**, Photon decay curves (blue dots) using a mono-exponential **(E_1, F_1)** or a bi-exponential **(E_2, F_2)** equation (red) and associated fitting residuals (black) extracted from pixels indicated respectively by a red and a green arrow in (C). Scale bar, 5 μm.

did not lead to a proper estimation of individual lifetime and proportions, and resulted in higher instability of the fitting algorithm. When a higher number of photons was collected (Fig. 4, cell No. 3, $\sim 4.10^4$ photons per curve), a bi-exponential fit was needed to calculate the proper mean lifetime and allowed the determination of proportion of interacting molecules ($\sim$60%), as well as lifetimes from both eGFP fluorescent species ($\sim$1.6 and $\sim$2.5 ns).

As shown in Figure 5, the use of Liχ also provided great improvement in the mean lifetime estimation. We observed a significant difference between mean lifetimes calculated from mono-exponential or bi-exponential fits which led to different interaction interpretations. Moreover, the examination of the residual shape of fitted pixel, revealed and emphasized that different models should be applied. For instance, the pixel pointed out by the red arrow (Fig. 5) required a bi-exponential fit whereas the one indicated by the green arrow suffered a mono-exponential fit. For these two pixels, mono and bi-exponential fits resulted respectively in a fluorescence lifetime of 2.22 ns and 1.76 ns for the red arrow and of 2.50 ns and 2.34 ns for the green arrow, corresponding to an error of 0.46 ns and 0.16 ns, respectively.

In summary, this easy-to-use procedure, based on the application of the $\Delta\chi^2$ fitting quality criterion within the Liχ algorithm provides an accurate fit model decision on a pixel by pixel basis, ensuring a robust interpretation of interacting populations, which would not be possible with a mono-model approach. This validated approach opens a new way towards interaction texture studies in heterogeneous biological samples, which mostly need quality fluorescence lifetime imaging analysis.

Acknowledgments

We kindly thank François Waharte and Nicolas Dross for providing biological applications and Jim Smith for his generous gift of the pCS-memb-mCherry plasmid.

Literature Cited

1. Wallrabe H, Periasamy A. Imaging protein molecules using FRET and FLIM microscopy. Curr Opin Biotechnol 2005;16:19–27.
2. Jares-Erijman EA, Jovin TM. FRET imaging. Nat Biotechnol 2003;21:1387–1395.
3. Sekar RB, Periasamy A. Fluorescence resonance energy transfer (FRET) microscopy imaging of live cell protein localizations. J Cell Biol 2003;160:629–633.
4. Gautier I, Tramier M, Durieux C, Coppey J, Pansu RB, Nicolas JC, Kemnitz K, Coppey-Moisan M. Homo-FRET microscopy in living cells to measure monomer-dimer transition of GFP-tagged proteins. Biophys J 2001;80:3000–3008.
5. Dong CY, French T, So PT, Buehler C, Berland KM, Gratton E. Fluorescence-lifetime imaging techniques for microscopy. Methods Cell Biol 2003;72:431–464.
6. Suhling K, French PM, Phillips D. Time-resolved fluorescence microscopy. Photochem Photobiol Sci 2005;4:13–22.
7. Waharte F, Spriet C, Heliot L. Setup and characterization of a multiphoton FLIM instrument for protein-protein interaction measurements in living cells. Cytometry Part A 2006;69:299–306.
8. Sillen A, Engelborghs Y. The correct use of "average" fluorescence parameters. Photochem Photobiol 1998;67:475–486.
9. Peter M, Ameer-Beg SM, Hughes MK, Keppler MD, Prag S, Marsh M, Vojnovic B, Ng T. Multiphoton-FLIM quantification of the EGFP-mRFP1 FRET pair for localization of membrane receptor-kinase interactions. Biophys J 2005;88:1224–1237.
10. Pelet S, Previte MJ, Laiho LH, So PT. A fast global fitting algorithm for fluorescence lifetime imaging microscopy based on image segmentation. Biophys J 2004;87:2807–2817.
11. Marquardt DW. An algorithm for least-squares estimation of non linear parameters. J Appl Math 1963;11:431–441.
12. Ritschard G, Zighed DA. Goodness-of-fit measures for inductions trees, In: Zhong N, Ras ZW, Tsumo S, Suzuki E editors, Foundations of Intelligent Systems. ISMIS03, LNAI 2871, Berlin: Springer; 2003. pp 57–64.
13. MacKay DJC. Information Theory, Inference, and Learning Algorithms. In: Press CU, editor. Cambridge: Cambridge University Press; 2003.
14. Myung IJ. The importance of complexity in model selection. J Math Psychol 2000; 44:190–204.
15. Wasserman L. Bayesian model selection and model averaging. J Math Psychol 2000; 44:92–107.
16. Zhong H, Wu X, Huang H, Fan Q, Zhu Z, Lin S. Vertebrate MAX-1 is required for vascular patterning in zebrafish. Proc Natl Acad Sci USA 2006;103:16800–16805.
17. Larson DR, Gosse JA, Holowka DA, Baird BA, Webb WW. Temporally resolved interactions between antigen-stimulated IgE receptors and Lyn kinase on living cells. J Cell Biol 2005;171:527–536.
18. Leonhardt H, Rahn HP, Weinzierl P, Sporbert A, Cremer T, Zink D, Cardoso MC. Dynamics of DNA replication factories in living cells. J Cell Biol 2000;149:271–280.
19. Monier S, Jollivet F, Janoueix-Lerosey I, Johannes L, Goud B. Characterization of novel Rab6-interacting proteins involved in endosome-to-TGN transport. Traffic 2002;3:289–297.
20. Wilcke M, Johannes L, Galli T, Mayau V, Goud B, Salamero J. Rab11 regulates the compartmentalization of early endosomes required for efficient transport from early endosomes to the trans-golgi network. J Cell Biol 2000;151:1207–1220.
21. Miserey-Lenkei S, Waharte F, Boulet A, Cuif MH, Tenza D, El Marjou A, Raposo G, Salamero J, Heliot L, Goud B, Monier S. Rab6-interacting protein 1 links Rab6 and Rab11 function. Traffic 2007;8:1385–1403.
22. Rasband WS. ImageJ. Bethesda, MD: U.S. National Institutes of Health. 1997–2007; http://rsb.info.nih.gov/ij/.